Tracing Coffee Tabletop Traces

Jork Leiterer,[†] Franziska Emmerling,*[,†] Ulrich Panne,[†] Wolfgang Christen,[‡] and Klaus Rademann*[,‡]

BAM Federal Institute for Materials Research and Testing, Richard-Willstätter-Strasse 11, 12489 Berlin, Germany, and Institut für Chemie, Humboldt-Universität zu Berlin, Brook-Taylor-Strasse 2, 12489 Berlin, Germany

Received March 11, 2008. Revised Manuscript Received May 13, 2008

Crystallization processes under different conditions are of fundamental interest in chemistry, pharmacy, and medicine. Therefore, we have studied the formation of micro- and nanosized crystals using water−caffeine (1,3,7-trimethyl-1*H*-purine-2,6(3*H*,7*H*)-dione) solutions under ambient conditions as a relevant model system. When droplets of an aqueous caffeine solution evaporate and eventually dry on surfaces (glass, polystyrene, and polyester), stable "coffee tabletop" rings with a perimeter of typically 3 mm are formed after 20 to 50 min. Using a micro focus X-ray beam available at the BESSY μSpot-beamline, the fine structure of different caffeine needles can be distinguished. Unexpectedly, both crystal modifications (α- and β-caffeine) are present, but locally separated in these rings. Furthermore, AFM studies reveal the presence of even smaller particles on a nanometer length scale. To eliminate influences of surface irregularities from the crystallization process, acoustic levitation of liquid samples was employed. Such levitated droplets are trapped in a stable position and only surrounded by air. The solvent in an ultrasonically levitated drop evaporates completely, and the resulting crystallization of caffeine was followed *in situ* by synchrotron X-ray diffraction. In this case, the diffraction pattern is in accordance with pure α-caffeine and does not indicate the formation of the room temperature polymorph β-caffeine. Hence, our investigations open new vistas that may lead to a controlled formation of cocrystals and novel polymorphs of micro- and nanocrystalline materials, which are of relevance for fundamental studies as well as for pharmaceutical and medical applications.

Introduction

Despite the great variety of crystalline organic substances (polymorphs or solvatomorphs) applied in pharmacy and medicine,[1] detailed investigations of the early stages of crystal formation and stability on a nanometer and micrometer length scale are still rare. Understanding the kinetics and dynamics of dissolution as well as recrystallization phenomena is of increasing importance to control the formation of crystalline structures and their properties during preparation. A particularly attractive process that can be exploited for creating equilibrium and nonequilibrium crystalline phases of small and large biomolecules is the controlled evaporation of sessile or levitated droplets containing a molecular solute. The evaporation of sessile droplets on surfaces is a fascinating phenomenon in its own. Frequently this process results in hierarchically organized stains of the solute, which was demonstrated for large colloids in suspensions.[2] One of the best known examples is the famous ring deposit formed by coffee drops on a table top.[3] Comparable phenomena have been described for large molecules like DNA for instance.[4] Common to these systems is the formation of liquid crystals or lamellar structures. The formation of crystals was not observed in the context of drop deposits so far, which is reasonable considering the difficult crystal formation. Keeping in mind that a common coffee drop consists of approximately 10^{-4} mol/L of caffeine the question arises in which way the drying process affects the modification of the eventually formed crystallites. Our particular interest in the study of these processes is motivated by the observation of caffeine crystals after supercritical fluid expansions[5] and the astonishing fact that the crystal structure of the low and high temperature modifications of caffeine could be clarified only recently.[6,7]

Tracing the coffee stain phenomenon, a decade ago a detailed explanation of the underlying physics emerged,[3] although the ring formation phenomenon as such had been known for centuries. While the physical aspects of hydrodynamics of ring formation seem to be rather clear,[3,8–11] the chemical solute−solvent and solute−solvent−surface interactions during ring formation and its crystallographic implications have not been investigated so far. In addition to the two-dimensional crystallization process on surfaces, we present the results of 3D and time-resolved *in situ* studies, allowing a geometrically unrestricted crystallization in all of the three space dimensions. Starting with a solution of caffeine, the initiation of crystallization was followed up to the bulk product by means of wide-angle X-ray scattering (WAXS). To the best of our knowledge, this is the first detailed study of the crystallization of a small organic molecule in an acoustically levitated droplet detected by microfocus WAXS.

* Corresponding authors. (K.R.) Phone: +49 (0)30 20935561, fax: +49 (0)30 20935559, e-mail: klaus.rademann@chemie.hu-berlin.de; (F.E.) phone: +49 (0)30 81041133, fax: +49 (0)30 81041137, e-mail: franziska.emmerling@bam.de.

[†] BAM Federal Institute for Materials Research and Testing.

[‡] Humboldt-Universität zu Berlin.

(1) Brittain, H. G. *J. Pharm. Sci.* **2007**, *96*, 705–728.

(2) Deegan, R. D.; Bakajin, O.; Dupont, T. F.; Huber, G.; Nagel, S. R.; Witten, T. A. *Phys. Rev. E* **2000**, *62*, 756–765.

(3) Deegan, R. D.; Bakajin, O.; Dupont, T. F.; Huber, G.; Nagel, S. R.; Witten, T. A. *Nature* **1997**, *389*, 827–829.

(4) Smalyukh, I. I.; Zribi, O. V.; Butler, J. C.; Lavrentovich, O. D.; Wong, G. C. L. *Phys. Rev. Lett.* **2006**, *96*, 177801–4.

(5) Christen, W.; Geggier, S.; Grigorenko, S.; Rademann, K. *Rev. Sci. Instrum.* **2004**, *75*, 5048–5049.

(6) Lehmann, C. W.; Stowasser, F. *Chem.−Eur. J.* **2007**, *13*, 2908–2911.

(7) Derollez, P.; Correia, N. T.; Danede, F.; Capet, F.; Affouard, F.; Lefebvre, J.; Descamps, M. *Acta Crystallogr., Sect. B: Struct. Crystallogr. Cryst. Chem.* **2005**, *61*, 329–334.

(8) Andreeva, L. V.; Koshkin, A. V.; Letiedev-Stepanov, P. V.; Petrov, A. N.; Alfimov, M. V. *Colloids Surf., A* **2007**, *300*, 300–306.

(9) Yakhno, T. A.; Yakhno, V. G.; Sanin, A. G.; Sanina, O. A.; Pelyushenko, A. S. *Tech. Phys.* **2004**, *49*, 1055–1063.

(10) Hu, H.; Larson, R. G. *J. Phys. Chem. B* **2006**, *110*, 7090–7094.

(11) Elbahri, M.; Paretkar, D.; Hirmas, K.; Jebril, S.; Adelung, R. *Adv. Mater.* **2007**, *19*, 1262–1266.

10.1021/la800768v CCC: $40.75 © 2008 American Chemical Society
Published on Web 06/26/2008

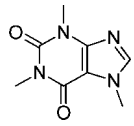

Figure 1. Scheme of caffeine (1,3,7-trimethylpurine-2,6-dione, $C_8H_{10}N_4O_2$).

Polymorphism of Caffeine. Crystallization has been described as one of the most difficult industrial operations to control.[12] The primary nucleation event is difficult to adjust reproducibly, and the competition between thermodynamic and kinetic factors affects the processes, which operate far from equilibrium. Consequently, different morphologies and crystal structures may result. The latter phenomenon is known as polymorphism, characterizing the propensity of a substance to crystallize into more than one crystal structure (see ref 13 and references therein). Polymorphism is a subject of great importance across the pharmaceutical, agrochemical, pigments, and fine chemical industries, having in common that the physical form of the products affects their properties, i.e. stability, color, dissolution, and bioavailability rate. Complex molecules, e.g. used by the pharmaceutical industry, tend to form polymorphs, which can have different solubility, different residence times in the body, and different therapeutic values. A related, quite common phenomenon is the formation of so-called solvatomorphs[1] or pseudopolymorphs.[13,14] These controversially discussed terms were coined to describe a compound obtained in crystalline forms that differ in nature or stoichiometry of included solvent molecules.

Crystallization in a supersaturated liquid requires the formation of a critical nucleus, which is also called a germ. In the framework of the classical nucleation theory (CNT),[15] crystallization is considered as a two-step process comprising first the formation of a germ (or nucleation) and second the subsequent growth of the crystal. Germ formation is a stochastic process and therefore susceptible to external influences. Insights into the crystallization process are needed to understand in detail the key physical processes which occur during nucleation, crystallization, and crystal growth, paving the way to a reliable formation of a desired polymorph. In this context, caffeine as a widely used food and pharmaceutical agent ($C_8H_{10}N_4O_2$ as shown in Figure 1) seems to be a promising starting point for our investigations.

Despite the industrial importance and wide use of the molecule, the crystal structure of the room and high temperature modification remained obscure for a long time. Surprisingly, the structures could only recently be characterized by solving the structure from powder-diffraction data.[6,7] The dynamically disordered high temperature phase α-caffeine (I) crystallizes in the trigonal space group *R*3*c*, whereas the room temperature phase *β*-caffeine (II) crystallizes in the monoclinic space group *Cc* with five crystallographically independent molecules in the asymmetric unit and a large *a* axis as depicted in Figure 2. When caffeine is crystallized from aqueous solutions, a monohydrate is built, whose crystal structure was first determined by Sutor in 1958.[16] The monohydrate tends to lose the solvent molecules and converts quantitatively to the anhydrous *β*-modification at room temperature.[17,18] This modification undergoes a phase transition when heated above 150 °C, yielding the α-polymorph.[7] After cooling to room temperature, the α-modification is metastable.

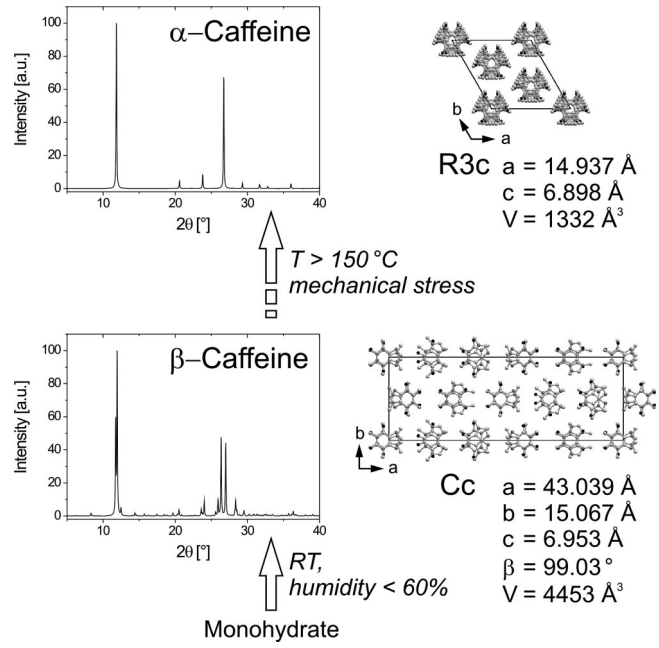

Figure 2. Polymorphs of caffeine and their structural relationship. Right: perspective drawings of the unit cells along [001] direction; left: corresponding calculated X-ray powder diffraction patterns indicating the differences.

Acoustic Levitation as an Analytical Tool. The surroundings of a sample, such as the wall of a glass capillary, may influence the structure and resulting physical properties of samples or their evaporating process as well. Furthermore, when an X-ray beam passes through a sample holder, it is scattered and contributes to the measured signal. Although this effect is mostly negligible for large sample volumes, the scattering of the sample holder makes it difficult to measure the scattering data precisely when the sample volume is small. Therefore, it is advantageous to measure the diffraction of samples without the presence of solid sample holders. An acoustic levitator allows a contactless sample positioning and eliminates the influence of the solid container wall. In addition, in situ-monitoring of solutions and suspensions during evaporation of the solvent is easily provided over a concentration range of 3 orders of magnitude. In a levitated droplet, the analyte mass is constant during evaporation and no losses occur. This is an advantage over cuvettes, where sorption processes on the walls have to be considered.

Working at an oscillating frequency of 58 kHz, a piezoelectric vibrator acts as an ultrasonic radiator (sonotrode, Figure 3). A standing acoustic wave is generated between this sonotrode and a concentrically adjusted reflector at a distance of some multiple of half the wavelengths. In several sound pressure nodes of this wave, as a result of axial radiation pressure and radial Bernoulli stress, liquid and solid samples can be placed and held in a levitated position without contact. Levitated samples have a typical volume of 5 nL to 5 μL (corresponding to a diameter of 0.2−2 mm). No other constraints on the sample such as magnetic or dielectric properties are relevant for acoustic levitation.

A droplet of a saturated aqueous solution of caffeine with a volume of about 4 μL was placed and levitated into the middle

(12) Paul, E. L.; Tung, H. H.; Midler, M. *Powder Technol.* **2005**, *150*, 133–143.
(13) Threlfall, T. L. *Analyst* **1995**, *120*, 2435–2460.
(14) Nangia, A.; Desiraju, G. R. *Chem. Commun.* **1999**, 605–606.
(15) Adamson, A. W. *Physical Chemistry of Surfaces*, 5th ed.; John Wiley & Sons Inc.: New York, 1990.
(16) Sutor, D. J. *Acta Crystallogr.* **1958**, *11*, 453–458.
(17) Pirttimaki, J.; Laine, E.; Ketolainen, J.; Paronen, P. *Int. J. Pharm.* **1993**, *95*, 93–99.
(18) Griesser, U. J.; Szelagiewicz, M.; Hofmeier, U. C.; Pitt, C.; Cianferani, S. *J. Therm. Anal. Calorim.* **1999**, *57*, 45–60.

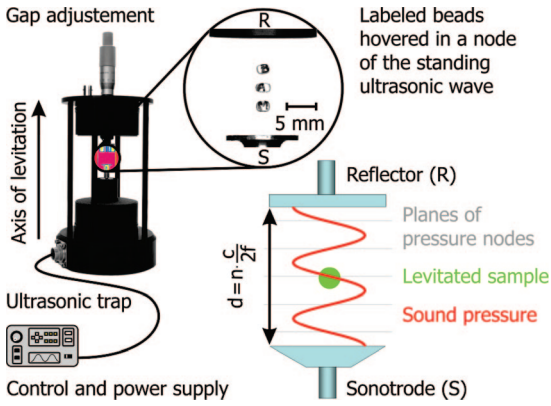

Figure 3. The acoustic trap and the principle of acoustic levitation (schematically).

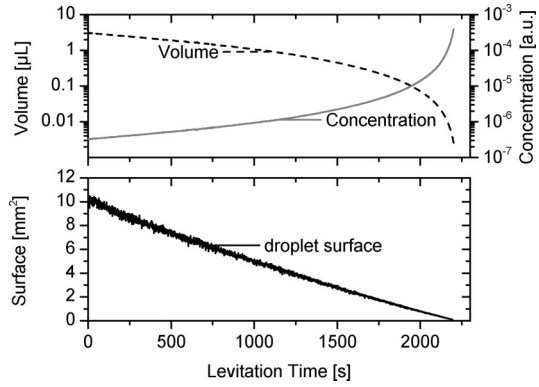

Figure 4. Measured decrease of volume and correlated increase of concentration as characteristic progress during evaporation, taking a levitated droplet of water as an example (upper part). Nearly linear decrease of the surface as a function of levitation time shows significant noise because of the method of determination (lower part).

wave node. The ambient air temperature was (298 ± 1) K. The sample persists in a fixed position during the measurement, even after evaporation of the solvent. The position stability of the droplet, measured as a displacement smaller than 20 μm, allowed more than 1 h data acquisition time by WAXS. The finally dry and solid sample was caught directly and stored in a container for later analysis by AFM and SEM.

Dynamics of Droplet Evaporation. Levitated samples are only surrounded by a gaseous environment, e.g. air. From the beginning of levitation the droplet's volume decreases gradually due to evaporation of the solvent and allows the study of phenomena such as aggregation in a dynamic and continuous fashion. The temporal evolution of the drop size is directly related to the concentration during the evaporation process. To monitor the size and shape of levitated droplets contactless is thus critical. Because of evaporation, the volume of levitated droplets decreases nonlinearly over time, but the surface shrinks nearly linearly over time (Figure 4). Evaporation processes of acoustically levitated droplets have been studied by several authors before.[19–22] Density gradients in the gaseous environment cause compensation streams which influence the process of evaporation.[23] For moderate sound pressures, which do not squeeze substantially the spherical form of the droplet, the progress of evaporation is

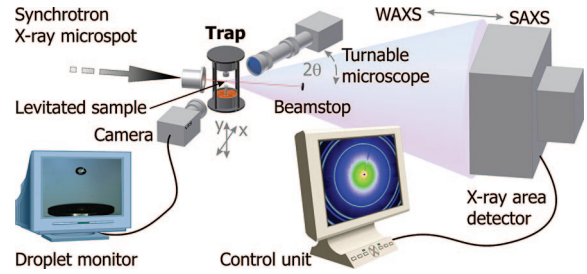

Figure 5. Sketch of the experimental setup for X-ray scattering experiments (WAXS and SAXS) with the ultrasonic levitator (trap) as a sample holder in its center.

quantitatively ascertainable.[23] The oscillation of a droplet and its surface can be described theoretically, and the influence on the evaporation progress was found to be negligible.[24,25] Nonetheless, a high sound pressure during crystallization in an acoustic levitator can exert influence on the resulting form of crystals because of shear stress in the levitated drop.[26] The influence of ultrasonic forces causes measurable warming of the pole of solid samples of a few degrees K. In the case of liquids no warming of the pole is quantifiable because of thermal convection and is assumed to be negligible.[27] As a first proof of the suitability of acoustic levitation as an technique for X-ray scattering, the crystallization of NaCl from aqueous solution was monitored *in situ*.[28]

To monitor the concentration of the levitated sample, different methods for determining size and shape of levitated droplets have been developed and compared recently.[29] For this purpose of contactless measurement optical methods are ideal. Illuminating the droplet with a telecentrical infrared flashlight generates a shadow due to the strong absorption of the solvent (water) in the infrared region at $\lambda = 880$ nm. The rotational symmetry around the axis of levitation allowed precise calculation of droplet volume from the cross sectional area (area of the shadow). Briefly, the second Guldinus theorem states that the volume of a solid of a revolution generated by rotating a plane figure about an external axis is equal to the product of the area of this figure and the distance traveled by its geometric centroid. The first Guldinus theorem declares analogously the determination of the surface. It is important to note that air convections due to the acoustic field induce an internal mixing of the liquid droplet and, therefore, homogenize continuously the material inside the droplet. This prevents concentration and temperature gradients from the center to the surface of the droplet when the solvent evaporates from the surface. This is in contrast to 2D-experiments on solid surfaces, where surface roughness and concentration gradients become relevant.

Experimental Section

Sample Preparation and Characteristics. Caffeine p.a. was purchased from Fluka (Buchs, Switzerland) and used without further purification. The X-ray diffraction (Bruker AXS, D5000, Cu Kα radiation) pattern of this sample indicates that it consists solely of β-polymorph. Eleven mg of caffeine were dissolved in 8 mL of deionized H_2O as stock solution. One droplet of about 4 μL with

(19) Lierke, E. G. *Acustica* **1996**, *82*, 220–237.
(20) Welter, E.; Neidhart, B. *Fresenius J. Anal. Chem.* **1997**, *357*, 345–350.
(21) Santesson, S.; Nilsson, S. *Anal. Bioanal. Chem.* **2004**, *378*, 1704–1709.
(22) Schiffter, H.; Lee, G. *J. Pharm. Sci.* **2007**, *96*, 2274–2283.
(23) Yarin, A. L.; Brenn, G.; Kastner, O.; Rensink, D.; Tropea, C. *J. Fluid Mech.* **1999**, *399*, 151–204.
(24) Yarin, A. L.; Weiss, D. A.; Brenn, G.; Rensink, D. *Int. J. Multiphase Flow* **2002**, *28*, 887–910.
(25) Rensink, D. Dissertation, Universität Erlangen-Nürnberg, Erlangen, 2004.
(26) Sacher, S.; Krammer, G. *Chem. Ing. Tech.* **2005**, *77*, 290–294.
(27) Tuckermann, R.; Bauerecker, S.; Cammenga, H. K. *Int. J. Thermophys.* **2005**, *26*, 1583–1594.
(28) Leiterer, J.; Leitenberger, W.; Emmerling, F.; Thünemann, A. F.; Panne, U. *J. Appl. Crystallogr.* **2006**, *39*, 771–773.
(29) Leiterer, J.; Emmerling, F.; Thünemann, A. F.; Panne, U. *Z. Anorg. Allg. Chem.* **2006**, *632*, 2132.

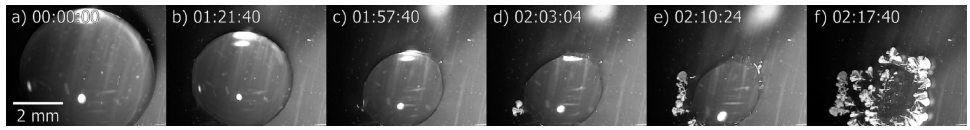

Figure 6. Sessile drop of caffeine solution on a polystyrene surface is evaporating under ambient conditions. The time stamp indicates the elapsed period after the droplet was deposited on the support.

known concentration of 7×10^{-3} mol/L was placed on a substrate or manually injected into the acoustic levitator by a common Eppendorf pipet (size 0.5−10 μL, Eppendorf, Germany). As exploratory substrates for contact surfaces, we used materials like glass (Th. Geyer, Berlin) and polyester film (Carl-Roth GmbH, Karlsruhe). All substrates were cleaned mechanically and used with their native surfaces.

Wide-Angle X-Ray Scattering (WAXS). The X-ray scattering experiments were performed using the μSpot beamline at BESSY. The focusing scheme of the beamline is designed to provide a divergence <1 mrad (horizontally and vertically) and a beam diameter of roughly 20 μm at a photon flux of 1×10^9 s^{-1} at a ring current of 100 mA. The experiments were carried out employing a wavelength of 1.00257 Å. The data obtained were corrected for background scattering. In case of levitated droplets, the scattering from pure solvent was measured and used for background correction. Microbeam diffraction using synchrotron radiation enables the local mapping of three-dimensional crystallite orientation in the sample. The data were processed and converted into diagrams of scattered intensities versus scattering vector q or scattering angle 2θ employing the computer program FIT2D.[30]

The scattering vector q is defined in terms of the scattering angle θ and the wavelength λ of the radiation (1.00257 Å) thus

$$q = \frac{4\pi}{\lambda} \sin \theta \qquad (1)$$

In the case of a large irradiated sample volume (many particles), the observed powder diffraction rings appear homogeneous while for a small sample volume the powder rings are spotty. For homogeneous Debye−Scherrer-rings the intensity as a function of the ring radius can be measured by scanning a narrow stripe of the image in radial direction. The resulting intensity versus ring radius is equivalent to data collected in a conventional powder diffraction experiment with a point detector mounted on the 2θ arm of a goniometer. If the same procedure is applied to inhomogeneous or discontinuous Debye−Scherrer-rings, intensities are dependent on the direction of the radial scan. To get reliable intensities, averaging over several radial scans taken along different azimuthal directions or over larger continuous segments of the Debye−Scherrer-rings are needed.

Atomic Force Microscopy (AFM). Pictures of dried caffeine sample at surfaces were taken by the atomic force microscope "Nanosurf Mobile S" (Nanoscience Instruments, Inc.). In order to exclude AFM artifacts (e.g., electrical line noise), a battery-powered system was used. For the purpose of eliminating actively acoustic noise we operated the AFM on a vibration isolated experimental board (Halcyonics, Inc.).

The multimode AFM, equipped with two different scan head types, a large and a high resolution scan head, allows for maximum xyz scan range of 110 × 110 × 22 μm and 10 × 10 × 1.8 μm, respectively. The capability of using the microscope in the dynamic force mode permits noninvasive imaging of the fragile nanostructures. Standard silicon tapping cantilevers (Pointprobe - Silicon SPM Sensors, Nanoworld, Inc.) were used with a typical force constant of 48 N/m and a thickness of 7 μm, a length of 225 μm, and a width of 38 μm, yielding a resonance frequency of about 190 kHz. The probe has a nominal tip radius of curvature of 10 nm. The instrument was fine-tuned and calibrated by using a standard calibration grating (xy periodicity of 10.0 μm, z height of 119 nm). All images were acquired in tapping mode.

Scanning Electron Microscopy (SEM). The imaging of desiccated samples of caffeine was performed on a Zeiss DSM 940. The acceleration voltage was fixed at 10 kV, and the working distance was 7 mm. Samples were fastened with conductive carbon tabs on aluminum sample holders. For better conductivity, the samples were coated with 10 nm of gold using a Baltec MED020 sputtering system. As required, an additional conductivity line was prepared by means of a silver finish.

Results and Discussion

Evaporation of Caffeine Droplets on Surfaces. All drying experiments performed on surfaces led to ring-like stains which can easily be explained by the coffee ring effect.[3] This physical effect can be observed on many different surfaces. We have checked polyester, polystyrene, and glass surfaces. To follow the evaporation process visually in detail a colored polystyrene surface was chosen because of its high contrast in light microscopy. On polystyrene surfaces sessile droplets were formed with an initial contact angle of (98 ± 2)° for water and (88 ± 1)° for aqueous caffeine solution. The polystyrene surface can be described by a root-mean-square (rms) value for the roughness R_{rms} = (3.5 ± 1.5 μm) (repeated AFM measurements of an area of typically 100 μm × 100 μm). Even for smaller areas (40 μm × 40 μm) the roughness is also on the order of (3.5 ± 1.5 μm). It is therefore reasonable to suggest that this surface roughness may influence the crystal formation process. The typical evaporation sequence of an aqueous caffeine solution, monitored by light microscopy, is presented in Figure 6. To trace the evaporation process, an optical microscope (DM-143, Motic, Inc.) with 10 times magnification and a video camera system (PAL, Motic Images Plus 2.0) was used.

Starting with an initial concentration of 7×10^{-3} mol/L, the evaporation process of the sessile drop at ambient conditions (T = 300 K, relative humidity RH ≈ 60%) takes about 2 h. The formation of the final deposits from the supersaturated solution typically lasts 10 min. As long as the droplet evaporates, the perimeter (contact line) diminishes continuously. It is fixed for a few seconds at a pinning point and continues to shrink again. During this process, surfaces of minimum area subject to constraints on the location of their boundary, so-called minimal surfaces, are developed.[31] As long as the droplet volume decreases, the concentration increases until suddenly a growth of needles starts pointing radially away from the contact line (see dotted line in Figure 7a).

Once the contact line is pinned (Figure 7a) material is deposited along the border (7b). Thereafter, entities start growing from each pinning point (Figure 7c−e) passing the primary contact line. This crystallization process continues until the supply of material is eventually disrupted (Figure 7f). In Figure 7d the crystals grown around the pinning point are shown in detail. Finally, the resulting crystal bundles are fixed on the polystyrene surface and cover a sector of circle up to 90° around the pinning point.

(30) Hammersley, A. P.; Svensson, S. O.; Hanfland, M.; Fitch, A. N.; Hausermann, D. *High Pressure Res.* **1996**, *14*, 235–248.

(31) Gennes, P. G. D.; Wyart, F. B.; Quere, D. *Capillarity and Wetting Phenomena Drops, Bubbles, Pearls, Waves*; Springer: New York, 2004.

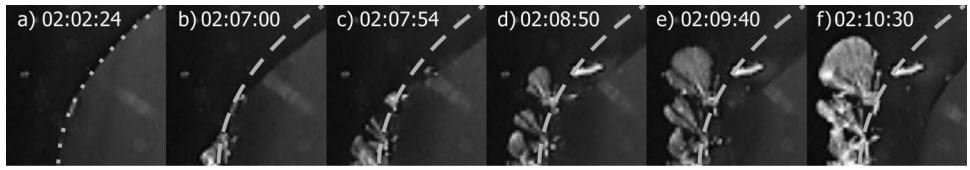

Figure 7. Microscope images of growing crystallites with the origin in a pinning point of the contact line. Magnification of the upper left pinning points described above in Figure 6. The contact line (dotted line) moves continuously to the inner region of the droplet and stops before the deposition starts. The changes throughout the process are evident comparing the droplet border with the initial contact line (dashed line).

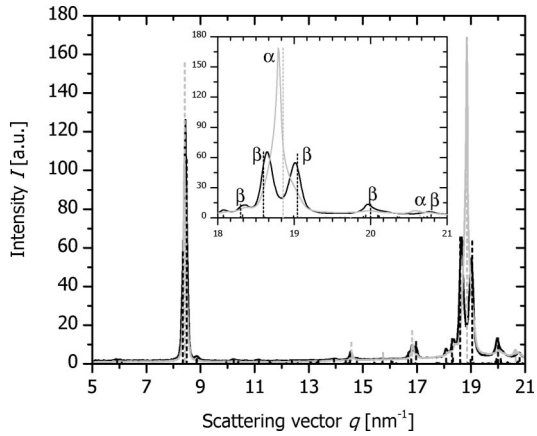

Figure 8. Caffeine crystallized from aqueous solution on the surface of a polyester film. For comparison, theoretical data from Cambridge Structural Database (CSD[32]) are indicated: High temperature (HT) α-phase (solid gray line) and room temperature (RT) β-phase (solid black line). Measurements of two different regions of the sample indicated by gray and black dashed lines. The inset highlights the scattering vector region between 18 to 21 nm^{-1}.

Facing the possible formation of rings we restricted our investigations to small droplets leading to tiny deposits with diameters of about (400 ± 50) μm and a typical mass of 145 × 10^{-9} g. A typical single droplet with a volume of 4 μL of an aqueous solution of caffeine was dried on the surface of a transparent polyester film. The initial contact angle of water (94 ± 1)° is reduced to (87 ± 4)° for the aqueous caffeine solutions indicating the weak activity of caffeine as a surface active agent (surfactant). The surface morphology of the polyester film can be described by a roughness R_{rms} = 4.6 μm (repeated AFM measurements of an area of typically 100 μm × 100 μm). This sample support was chosen because of its surface morphology, low background signal, and its low X-ray absorption. After evaporation of the droplets, small deposits with irregular boundaries were left on the surface. The resulting small apparently homogeneous stains typically exhibited a diameter smaller than 500 μm. A closer investigation of these stains was carried out by scanning experiments with a 20 μm X-ray beam. The recorded diffraction patterns indicate clearly the presence of both caffeine modifications, the room temperature (β), and the high temperature modification (α) in spatially separated regions.

As shown in Figure 8 the existence of two phases can be distinguished easily, considering the most intense reflexes at q = 8.5 nm^{-1} and 19 nm^{-1}. Here, the diffractogram of the α-phase exhibits a single reflex at q = 18.8 nm^{-1}, whereas the diffractogram of the β-phase displays two reflexes at q = 18.6 nm^{-1} and 19.0 nm^{-1} (inset of Figure 8).

Keeping in mind that the measured enthalpy of phase transition of the β-polymorph to the α-polymorph amounts to 4.1 kJ/mol at 420 K,[33,34] it can be expected that both modifications are present in the crystalline deposits. The spatial resolution achieved is about several microns, comparable to the roughness of the surface. Since the surface roughness establishes independent compartments the formation of both phases is reasonable. Each tiny compartment provides different conditions which finally direct the crystallization process to one of the modifications. The experiment described above was repeated on glass surfaces providing a more homogeneous and better defined surface roughness with R_{rms} = 5 nm (AFM measurements for an area of typically 100 μm × 100 μm at several locations). The contact angle increases from (45 ± 3)° of water to (59 ± 4)° of aqueous caffeine solution, in contrast to a reduction of the contact angle at the surface of the polyester film.

From a sample deposited on a glass substrate, different regions were selected by their specific morphologies and classified into the following four categories: The inner homogeneous region (D), radial arranged needles (A), origin of a bunch of needles (B), and a single needle (C). The examined regions are indicated in Figure 9. After having passed the glass, the X-ray beam irradiates the caffeine deposits.

From the obtained well defined X-ray diffraction patterns of all selected positions, a crystalline character of the caffeine deposits can be concluded. The diffraction patterns, gained from the inner part of the deposits D, show no pronounced reflexes and thus suggest an amorphous character of the inner region. The diffraction patterns of the regions A−C were all assigned unambiguously to the α-phase of caffeine as presented exemplary for region C in the inset of Figure 9.

Preferred Orientation of Crystal Growth. The caffeine crystallites are orientated, as it can be assumed from the microscope image in the right part of Figure 9. The question arises if this visible orientation is correlated to a preferred orientation of the crystallites. A broader azimuth distribution of the diffracted intensities is an indication of a low crystallite's alignment. On the other hand, a sharp distribution indicates a high degree of orientation. Figure 10 shows the diffraction pattern of the upper part of a needle wisp (region A). From the microscopic and the SEM images (Figure 12 *vide infra*) it is apparent that the region consists of aligned crystal needles covering an angle of approximately 60°. Consequently the 2D diffraction pattern (Figure 10) resembles a pole figure with two defined regions of reflexes. The bigger arc-like sector represents directly the circular arrangement of the needles, expressing the observed orientation distribution. Intensities obtained in this sector (from −11 to −46°, right bottom corner) are related to the 012-reflex (q = 18.9 nm^{-1} and d = 3.33 Å, respectively). The smaller sector (between gray dotted lines in the region of 54−70°) perpendicular to the first one stems from reflections along the needle direction, apparently consisting of more uniform scattering objects. The azimuthally integration of this sector leads to scattering intensities which can

(32) CSD, Cambridge Structural Database The Cambridge Crystallographic Data Centre, 12 Union Road, Cambridge, CB2 1EZ, UK.

(33) Bothe, H.; Cammenga, H. K. *J. Therm. Anal.* **1979**, *16*, 267–275.

(34) Epple, M.; Cammenga, H. K.; Sarge, S. M.; Diedrich, R.; Balek, V. *Thermochim. Acta* **1995**, *250*, 29–39.

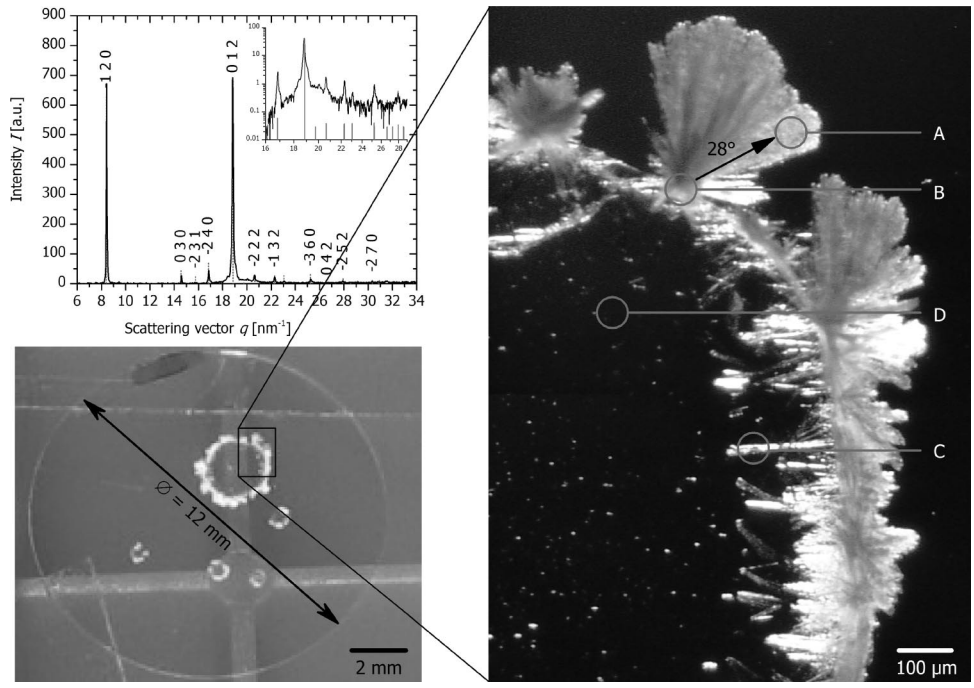

Figure 9. Caffeine on the surface of a glass slide (12 mm in diameter, bottom left) with selected positions (A−D, see microscope image on the right). Exemplarily experimental data obtained from region C were compared with indexed diffraction pattern of the α-modification (extracted from ref 7, top left).

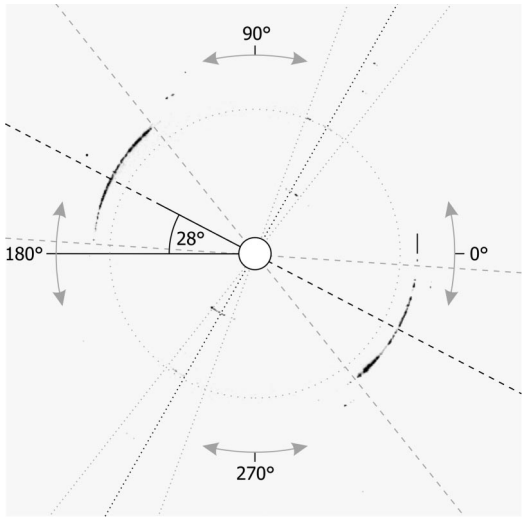

Figure 10. Diffraction pattern where mean intensity distribution can be divided in two groups (between dashed lines from top left to bottom right and dotted lines from bottom left to top right). The means of distributions are marked (black lines). The marked angle is between the dashed black line and the horizontal line (at 180° and 0°, respectively).

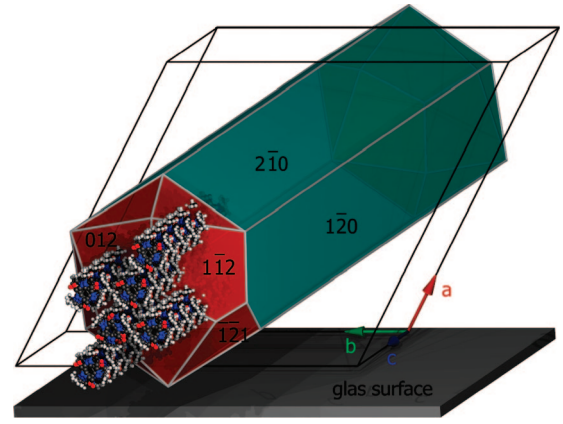

Figure 11. Crystal structure and BFDH morphology (with labeling of the facet edges) of α-caffeine. The surface of glass is in the plain of the *b*−*c*-axis.

be related to the ($\bar{1}$20), ($\bar{2}$22), and ($\bar{1}$30) reflexes of α-caffeine. The observed 2D reflection pattern can be explained based on the following model. The needle axis of the caffeine crystals is parallel to the crystallographic *c*-axis and the *a*-axis is parallel to the glass surface. This results in a perpendicular orientation of the ($\bar{1}$20) plane relative to the glass surface. Since the ($\bar{1}$20) and the (012) plane enclose an angle of 77° to each other, it is reasonable that the reflections of the (012) plane appear nearly perpendicular to those of the first sector.

The dashed black line crosses the horizontal line by an angle of 28°. Regarding the orientation of the diffraction pattern (Figure 10 along the direction, and Figure 9 with the opposite direction of incident radiation) it is not surprising that the determined angle of 28° represents exactly the visible angle of crystallite orientation. The lower diffraction intensities of the ($\bar{1}$20) plane compared to the (012) plane results from the orientation of the crystals. The Bravais Friedel Donnay Harker (BFDH) method was used for morphology prediction and calculation of crystal shaping faces of caffeine. Figure 11 presents the molecular model and the oriented needle of caffeine. The crystal is aligned in the direction of the *c*-axis which is in plane of the glass surface.

Electron microscopy provides deeper insights into the formed structures of interest and gives images of 100 times higher resolution compared to visible light microscopy. SEM images of the marked positions of Figure 9 are presented in Figure 12.

The positions supposed to consist of single needles are actually built by a bundle of small needles. All SEM images are in good agreement with the observations during the evaporation by optical microscopy. The outer region (Figure 12A) is dominated by ordered needles, which grew starting from the former contact line. These outer parts are formed rapidly in the first stages of

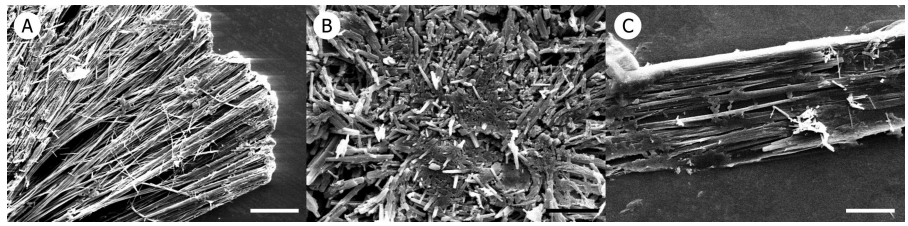

Figure 12. SEM images of aligned needles of caffeine. Positions (A, B, and C) as described above. Magnifications are 370 (A), 2000 (B), and 1850 (C). Scale bar in A: 50 μm, B: 10 μm, and C: 10 μm.

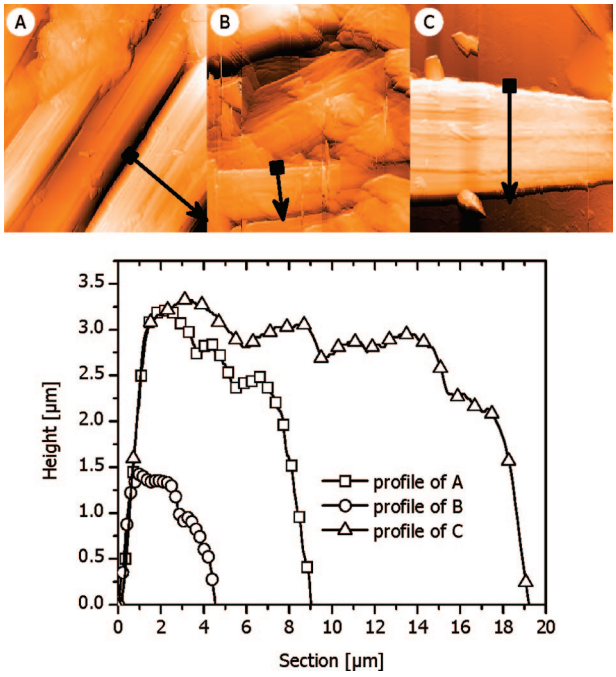

Figure 13. AFM images of different parts of crystallized caffeine on glass surface where A represents 20 × 20 μm, B 20 × 20 μm, and C 40 × 40 μm. A cross-sectional view for the line drawn (arrow) is included for each image. Every 10th point is marked by the symbol square (profile of A), circle (profile of B), and triangle (profile of C).

crystallization characterized by the continuous material transport from the inner part of the droplet. As the material transport decreases, small irregularly arranged needles with a size of approximately 10 μm length are formed at the origin of the needle bundle (Figure 12B). The needle built in the inner part of the former droplet (Figure 12C) is composed of multiples of aligned needles. Remarkably, the needle orientation parallel to the glass surface is in agreement with the model as visualized in Figure 11.

AFM images give access to the heights of the structures. The diameter of the material at the border of the ring is determined to 35 μm. In contrast, smaller diameters from several hundred nanometers up to 1 μm where found from the cubic rods in Figure 12B. These needles have a mean length of a few microns and are not aligned like the needles in the region C (Figure 12). There they are more or less ordered in a parallel alignment with lengths up to 300 μm.

On indicated lines in the upper part of Figure 13 cross-sectional height data were analyzed for each position A, B, and C corresponding to Figure 9 (WAXS) and Figure 12 (SEM). The diagram in the lower part shows the related height profiles and provides exemplarily a diameter for the marked structures (black arrows).

The relation of diameters analyzed by AFM images of point A (9 μm), B (4.5 μm), and C (19 μm) is in good agreement with the estimated median size of structures in SEM images. Additionally, the size of the crystallites can be evaluated from diffraction patterns as obtained via X-ray diffraction (XRD, see below).

Caffeine Evaporation in an Acoustic Trap. In order to exclude any influences of solid surfaces (contaminations, contact line pinning, and ion exchange processes), the crystallization of caffeine from an aqueous solution was followed *in situ* in an acoustic levitator. Hence, a three-dimensional crystallization process is induced by solvent evaporation. Typically, during 1 h the solvent water was evaporated. As shown in Figure 14 the transparent droplet ($\varnothing = 1.7$ mm) decreases and changes to a white small bulk ($\varnothing \approx 0.2$ mm). By the assumption of a sphere, this bulk corresponds to a final volume of 0.4 μL and a concentration of 7×10^{-2} mol/L.

During levitation experiments, 45 diffraction patterns were collected within a time interval of 60 s including an exposure time of 40 s. Toward the end of the experiment, integration times of 120 and 300 s were applied to achieve a better signal-to-background ratio. At the beginning of the experiment no crystalline species are formed as the absence of Bragg reflections in the first two-thirds of the displayed diffractograms indicates (Figure 15). The first detectable reflexes are those of the $(\bar{1}20)$ and the (210) plane of the high temperature (α) modification of caffeine. The succeeding patterns already display the complete diffractogram of α-caffeine.

The Debye−Scherrer rings observed in the experiment are continuous, which can be explained by the long averaging through the rotation of the levitated droplet. Astonishingly, no other phase was formed throughout the experiment, and the crystallization process leads to a single product. Compared to the experiments carried out on the surfaces, the continuous diffusion and mixture processes prevent a continuous growth of germs. Therefore, no crystals of adequate size for XRD experiments are built. The process of germ formation and dissolution persists until the saturation in the droplet reaches a critical value, and crystallization starts for the entire sample volume at once. At this point, the formation of the metastable phase α-caffeine is energetically favored.

The two-dimensional (2D) WAXS patterns of caffeine in the trap and crystallized on a glass surface are shown in Figure 16. Both scattering images can be distinguished easily: Rings from caffeine on glass show nonisotropic Laue-rings, as the number of scattering crystallites is too small for a sufficient statistic distribution of scattering intensities. In contrast, the scattering intensities from a levitated droplet document the existence of randomly orientated crystallites contributing to isotropic Laue-rings. As a levitated droplet rotates and wobbles randomly around its equilibrium position with an uncertainty of about 20 μm, a small number of caffeine crystallites can be detected with an integration time of 60 s because of this spatial averaging. We conclude that an acoustic levitator improves the quality of scattering images leading to a higher degree of isotropy.

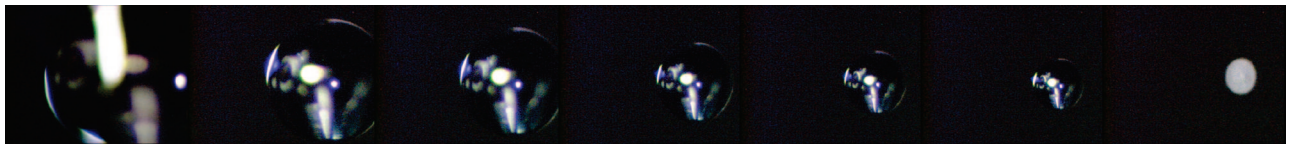

Figure 14. Continuous decrease of the droplets' size and the transition from the liquid to the solid phase during a levitation time of 63 min. Droplet is diminishing in diameter from 1.7 to 0.2 mm.

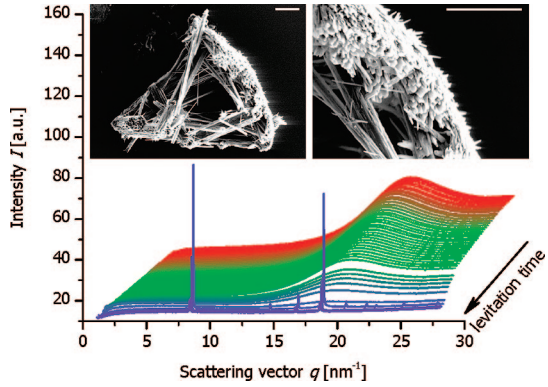

Figure 15. Scattering patterns recorded during crystallization of caffeine in water (bottom). SEM images from the dried bulk (left) and enlarged detail (right). Both scale bars are 20 μm, and the levitation time is 50 min.

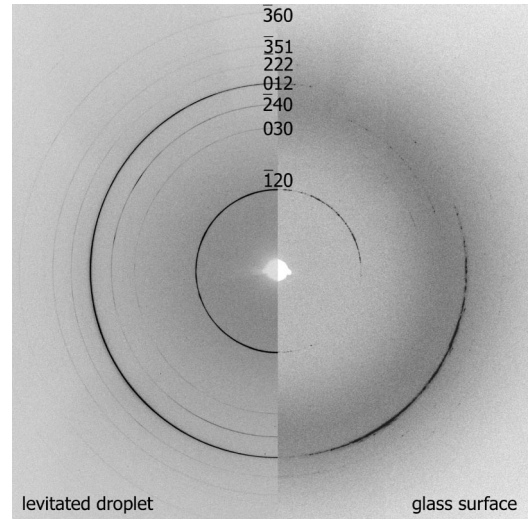

Figure 16. Diffraction rings of caffeine in droplet (left) and caffeine on glass (right) with corresponding Miller indices.

Size of Crystallites. To gain further insights into the crystallization process, the size of crystallites was studied. A crystallite is the smallest part of sample with the same ordered crystalline structure. The size of the crystallite correlates with the width of its Bragg reflexes. Bearing in mind that diffraction line broadening can be ascribed to several phenomena such as small crystallite dimensions, lattice imperfection, and instrumental contributions, the Scherrer equation[35,36] can provide a rough estimate of the crystallite size. It correlates on a wavelength independent q scale the size of crystallites through the derivation of the defined scattering vector q with respect to θ. Equation 1 thus yields

$$\frac{\mathrm{d}q}{\mathrm{d}\theta} = \frac{\mathrm{d}}{\mathrm{d}\theta}\left(\frac{4\pi}{\lambda}\sin\theta\right) = \frac{4\pi}{\lambda}\cos\theta$$

$$\frac{\lambda}{2\mathrm{d}\theta\cos\theta} = \frac{2\pi}{\mathrm{d}q}$$

$$\frac{k\lambda}{w\cos\theta} = \frac{2\pi}{B_{\mathrm{int}}} = D_{hkl}, \qquad (2)$$

where k is a constant close to unity and w is the width on a 2θ scale. The width of a reflection is measured by its integral width B_{int} defined as

$$B_{\mathrm{int}} = \frac{\int_0^\infty I(q)}{I(q_{\mathrm{max}})} \qquad (3)$$

Using B_{int} allows the calculation of the crystallite size D_{hkl} independent of the shape of the reflection under consideration. In the case of our synchrotron X-ray diffraction pattern, the broadening caused by influences from beam divergence <1 mrad and beam diameter of 20 μm is negligible and will not be taken into account. This estimate is justified by the diffraction at corundum with a known crystallite size (D_{hkl}> 110 nm), which results in well defined Bragg reflexes.

Table 1. Measured Width of Reflexes and the Size of Crystallites Calculated Thereof[a]

regions marked in Figure 9	Δq [nm^{-1}]	XRD [nm]	SEM [μm]	AFM [μm]
A	0.076	41.2 ± 1	1 × 300	9.0 ± 0.5
B	0.11	28.4 ± 0.5	1 × 5	4.2 ± 0.5
C	0.026	120 ± 5	35 × 300	19 ± 0.5
droplet	0.068	46 ± 1	2 × 20−90	not done

[a] The sizes from SEM and AFM are shown for relation analogy and not directly comparable. A, B, and C mark the analyzed region of caffeine as described above.

The calculated minimal values of the mean crystallite size show a clear trend from 41 to 120 nm (Table 1). The crystallite sizes of the radially arranged crystallites (A) and of a single needle (C) differ by a factor of 3 and are slightly larger than those from the origin of needles (B).

The dimensions gained from SEM and AFM experiments are values for the physical size and therefore multiples higher than values calculated from XRD pattern. Consequently, the visible structures can be considered to consist of several crystallites. The minimum value for the mean size of caffeine crystallites obtained from an aqueous droplet was evaluated from the width of reflexes to 46 nm. It is therefore in the range of the size values for caffeine crystallites dried on a glass surface. Sizes from all methods show a clear trend (C > A > B). AFM analysis for A show half the size structures than for C whereas sizes for B are once more smaller. These relations draw a parallel with the sizes given from SEM images. Furthermore, the relation of sizes from SEM images correlate with the calculated mean size of crystallites. Here the mean size of C is three times higher than of A, and this is 45% higher than that of B.

(35) Scherrer, P. *Nachr. Ges. Wiss. Göttingen* **1918**, *2*, 98–100.
(36) Klug, H. P.; Alexander, L. E. *X-Ray Diffraction Procedures: For Polycrystalline and Amorphous Materials*, 2nd ed.; Wiley-Interscience: 1974; p 992.

Summary and Conclusions

In this work we describe the crystallization processes of caffeine on glass, polystyrene, and polyester surfaces (sessile droplet), as well as on gas−liquid interface (levitated droplet). The results of time-resolved investigations using an ultrasonic trap by means of wide-angle X-ray scattering (WAXS) are presented. For an investigation of the underlying processes, it is important to choose analytical methods providing information on the same length scale as the specimen under study. Consequently, our investigations cover μ-focus-WAXS analysis and AFM and SEM experiments to elucidate the crystallization of caffeine on different surfaces. As for experiments carried out on surfaces, the results corroborate our assumed model for the crystallization dynamics. The main features of the primarily two-dimensional crystallization process on surfaces can be described as follows. The first stage is characterized by a decrease of the sample volume together with the drop off of the pinning line. In the following the radial growth of caffeine crystallites starting at the former pinning line was observed. The final part of the process consists of a rapid evaporation leading to a fast deposit of material in the inner region of the caffeine rings. The findings are supported by the results obtained from the analysis of crystallite sizes by means of XRD, AFM, and SEM measurements. The outer parts of the caffeine rings consist of many caffeine crystals whereas the inner part and the center of the ring consist of fewer larger ones and nanocrystals, respectively. The experiments carried out on PE foil led to the spatially separated formation of both caffeine modifications whereas on glass surfaces the α-modification was formed. In comparison of these two substrates the differences most probably stem from the different surface roughness, allowing spatially independent crystallization processes in case of the PE foil and hence a statistic mixtures of α and β modification. In contrast, the uniform glass surface seems to provide equal conditions throughout the whole sample volume and leads to a monophasic product.

Surface irregularities of the sample holder do not only influence the crystalline modification. Moreover, they can involve preferential direction of growth. The transition from the primarily two-dimensional to a three-dimensional crystallization environment helps to clarify possible surface influences. In the case of the experiments carried out in suspended droplets the formation of a single crystalline phase (α-caffeine) was observed. Astonishingly, this experimental setup leads directly to the final phase, although appearance of different modifications throughout the process and in the final product seems to be reasonable. Furthermore, no hydrated caffeine modifications were detected. The crystallization of organic compounds starts with solute−solvent aggregates, containing solute−solvent, solute−solute, and solvent−solvent interactions. The entropic gain in eliminating solvent molecules from aggregates into the bulk solution, and the concurrent enthalpic gain in forming stable solute species, provides adequate driving forces for nucleation and crystallization, leading to unsolvated organic crystals. From an enthalpic point of view, the extrusion of solvent from the aggregates into the bulk can become disadvantageous when solvent molecules are attached to solute molecules via stronger interactions, i.e. hydrogen bonds. Consequently, the solvent molecules remain an integral part of the nucleating crystal. Therefore, the formation of a solvated crystal may be connected to an interruption of the sequence of events accompanying the crystallization of the unsolvated form. Apparently, the processes in the trap environment are entropically driven and lead exclusively to the formation of the unsolvated forms. The finally built crystalline phase is a kinetically controlled product. One possible explanation for these findings is that the equilibriums present in the trap lead to fast construction and deconstruction of different modification yet not allowing one of the phases involved to reach the critical volume necessary for detection by means of X-ray diffraction. At the beginning of the evaporation process the turbulences within the suspended droplet prevent the formation of local concentration differences, which are typically established at the walls of a vessel during a standard crystallization experiment.[12] This situation changes drastically at the end of the experiment where saturation conditions are reached for the entire sample volume at once. Successively, the crystallization process starts throughout the whole sample volume leading to metastable α-caffeine. The described conditions are totally different from those in experiments on polyester foil surfaces. Here, the surface morphology of the substrate leads to spatially separated crystallization processes on the substrate, resulting in individually differentiating crystallization conditions in the 5 μm compartments provided by the polymer substrate. Therefore it is reasonable that both caffeine modifications are detectable in this setup. According to our recent and previous[28,37] findings, the ultrasonic trap not only prevents surface effects, it also serves as a tool to influence the crystallization process leading to monophasic products.

Acknowledgment. We would like to thank Simone Rolf of BAM for technical assistance and Robin Meier of the Lise-Meitner school for preparing the AFM images. We thank Stephan E. Wolf (scholarship holder of Konrad-Adenauer-Stiftung) for assistance and Prof. Dr. W. Hofmeister (both from Johannes Gutenburg-University) for granting access to SEM facilities. Dr. A. Thünemann from BAM is acknowledged for critical reading of the manuscript. Dedicated to Professor Dr. Manfred Hennecke on the occasion of his 60th birthday.

LA800768V

(37) Wolf, S. E.; Leiterer, J.; Emmerling, F.; Tremel, W. **2008**, submitted for publication in *J. Am. Chem. Soc*.